Nematic ordering dynamics of an antiferromagnetic spin-1 condensate

L. M. Symes[1] and P. B. Blakie[1,2,*]

[1]*Dodd-Walls Centre for Photonic and Quantum Technologies, Department of Physics, University of Otago, Dunedin 9016, New Zealand*

[2]*Swinburne University of Technology, Sarawak Campus, School of Engineering, Computing and Science, Jalan Simpang Tiga, 93350 Kuching, Sarawak, Malaysia*

(Received 4 April 2017; published 5 July 2017)

We consider the formation of order in a quasi-two-dimensional antiferromagnetic spin-1 condensate quenched from an easy-axis to an easy-plane nematic phase. We define the relevant order parameter to quantify the spin-nematic degrees of freedom and study the evolution of the spin-nematic and superfluid order during the coarsening dynamics using numerical simulations. We observe dynamical scaling in the late-time dynamics, with both types of order extending across the system with a diffusive growth law. We identify half-quantum vortices as the relevant topological defects of the ordering dynamics and demonstrate that the growth of both types of order is determined by the mutual annihilation of these vortices.

DOI: 10.1103/PhysRevA.96.013602

I. INTRODUCTION

Spin-1 condensates [1–3] with antiferromagnetic interactions prefer to order into spin-nematic phases [4]. Such phases have a vanishing average spin density and are, instead, characterized by the nematic tensor $\mathcal{N}_{ab} = \frac{1}{2}\langle f_a f_b + f_b f_a\rangle$, where $f_{a\in\{x,y,z\}}$ are the spin matrices. The ground states of this system have an axially symmetric nematic tensor (uniaxial nematic) with a preferred axis (but not direction) characterized by a director $\vec{u}$ in spin space (i.e., $\vec{u}$ and $-\vec{u}$ are equivalent). Recently experimental evidence was presented for spin-nematic order in an antiferromagnetic condensate [5].

The concept of nematic order is typically discussed in the context of liquid crystals, where the order is associated with the orientation of long molecules. Indeed, many beautiful studies of phase transition dynamics and coarsening have been performed in liquid crystal systems (e.g., see [6–12]). A sudden change in conditions (e.g., temperature or pressure) is used to quench this system from an isotropic phase (unoriented molecules) to the nematic phase, and the formation of order and defect dynamics can be observed optically.

In this paper we develop a theory for the ordering dynamics (coarsening) of an antiferromagnetic spin-1 condensate. There has been considerable theoretical work on the coarsening dynamics of ferromagnetic spin-1 condensates [13–16], however, this area is largely unexplored in the antiferromagnetic system. Our interest is in the symmetry-breaking phase transition from an easy-axis (EA) phase (with $\vec{u}$ along the direction set by the external magnetic field) at positive quadratic Zeeman energy q to an easy-plane (EP) phase ($\vec{u}$ transverse to the external field) at negative q (see Fig. 1(d) and Refs. [17–21]). We consider a quench between these phases implemented by a sudden change in q, e.g., using microwave dressing (see [17,18,20]). Upon entering this new phase, the system breaks the continuous axial symmetry of the initial state by developing transverse spin-nematic domains. Here our interest lies in characterizing the dynamics of the phase transition, with particular emphasis on the late-time coarsening dynamics, that is, to understand the universal aspects of how small domains created after the quench anneal together to bring the system towards an ordered equilibrium state. To undertake this study we first discuss how the nematic order is characterized in a spinor condensate and develop an appropriate order parameter for the EP phase. Using numerical simulations we study how the EP order forms in the system. We demonstrate that the late-time coarsening behavior exhibits dynamical scaling with a diffusive domain growth law of $L(t) \sim [t/\ln(t)]^{1/2}$, where L is the size of the ordered domains and t is the time after the quench. We separately consider the superfluid order and show that it grows with an identical law to the spin-nematic order, in contrast to recent results for the ferromagnetic spin-1 system [22]. The order parameter growth is determined by the dynamics of half-quantum vortices (HQVs) in the system, and we verify that the number of these vortices scales as $L(t)^{-2}$, i.e., that coarsening proceeds by vortex-antivortex pairs mutually annihilating. Recent experiments have demonstrated that it is possible to measure HQVs in antiferromagnetic spin-1 condensates [23,24] due to their ferromagnetic cores [25]. Thus, measuring the HQV distribution as a function of the time after the quench could be a practical method for experiments to quantify the coarsening of this system. Alternatively, it may be possible to directly image [26,27] or probe [28] nematic properties of the condensate.

We note that the symmetries and defects of the EP phase are similar to those of a (two-component) binary condensate in the miscible regime. Indeed, work by Karl *et al.* [29] discussed the role of equivalent vortices in the ordering dynamics of a two-component system, although that work focused on understanding the emergence of power-law behavior in various momentum correlation functions and relating these to turbulence cascades.

The outline of the paper is as follows. In Sec. II we introduce the basic formalism for spin-1 condensates and consider how to quantify spin-nematic order. We discuss the EA-to-EP quench and introduce the relevant order parameter for this phase transition. In Sec. III we start by introducing the quasi-two-dimensional (quasi-2D) system, equation of motion, and simulation technique we use to study the quench dynamics. We present results for the evolution of various local densities and correlation functions that illustrate the early-time dynamics of the quench and show the emergence of EP order. We then focus on the late-time dynamics of the system and characterize the phase ordering dynamics. To do

*blair.blakie@otago.ac.nz

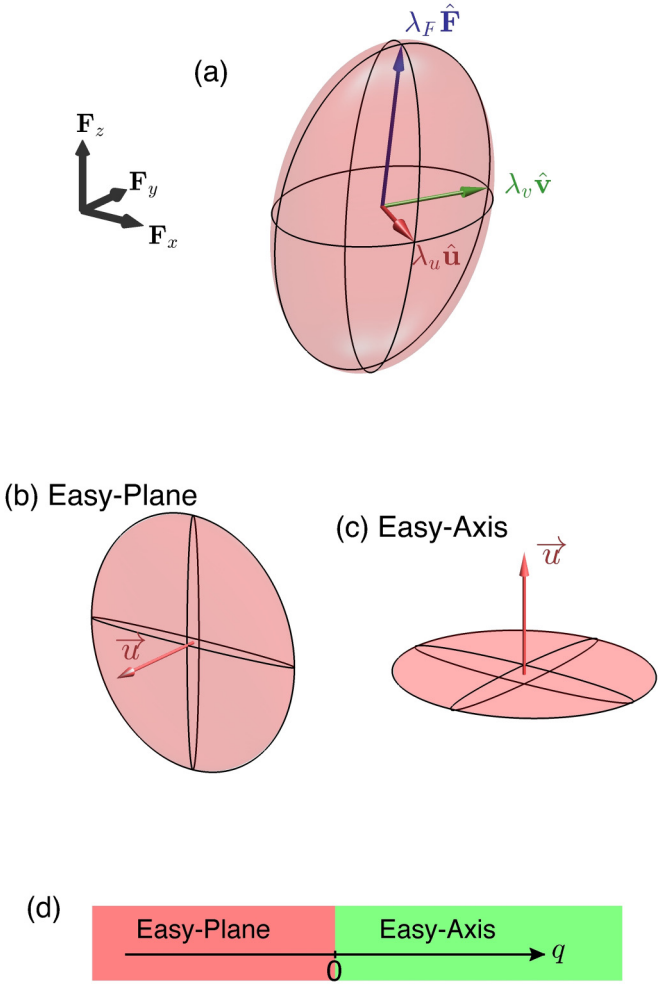

FIG. 1. (a) Representation of the nematic tensor $\mathcal{N}$ of a spin-1 state as an ellipsoid. The semiprincipal axes are along eigenvectors of $\mathcal{N}$ indicated by the unit vectors of $\{\vec{u},\vec{v},\mathbf{F}\}$, with the widths in these directions given by the corresponding eigenvalues $\{\lambda_u,\lambda_v,\lambda_F\}$. A polar state is a flat disk-shaped ellipsoid [see (b) and (c)] completely characterized by the director $\vec{u}$, with spin fluctuations maximized in the plane transverse to $\vec{u}$. (b) Easy-plane and (c) easy-axis cases of the polar state. (d) Ground-state phase diagram as a function of q. Note that the direction of the external magnetic field sets our z axis.

this we introduce correlation functions for the spin-nematic and superfluid order. We evaluate these using an ensemble of large-scale simulations, demonstrate correlation function collapse (dynamic scaling), and extract the relevant growth laws. Finally, we examine the role of HQVs and show that the average distance between vortices characterizes the growth of order. Then we conclude in Sec. IV.

II. FORMALISM

A. Spin-1 antiferromagnetic condensate

A spin-1 condensate is described by the spinor field

$$\boldsymbol{\psi} \equiv (\psi_1,\psi_0,\psi_{-1})^T, \tag{1}$$

where the three components describe the condensate amplitude in the spin levels $m = 1$, 0, and -1, respectively. The short-ranged interactions between atoms are described by the rotationally invariant Hamiltonian density

$$\mathcal{H}_{\rm int} = \frac{g_n}{2}n^2 + \frac{g_s}{2}|\boldsymbol{F}|^2. \tag{2}$$

The first term describes the density-dependent interactions, with coupling constant g_n, where $n \equiv \boldsymbol{\psi}^\dagger\boldsymbol{\psi}$ is the total density. The second term describes the spin-dependent interactions $g_s|\boldsymbol{F}|^2$, with coupling constant g_s, where $\boldsymbol{F} \equiv \boldsymbol{\psi}^\dagger\boldsymbol{f}\boldsymbol{\psi}$ is the spin density and $\boldsymbol{f} \equiv (f_x,f_y,f_z)$ are the spin-1 matrices. For the case $g_s > 0$, known as antiferromagnetic interactions, the condensate prefers to minimize the spin density to reduce the interaction energy. In addition to interactions, the (uniform) quadratic Zeeman shift,

$$\mathcal{H}_{\rm QZ} = q\boldsymbol{\psi}^\dagger f_z^2\boldsymbol{\psi}, \tag{3}$$

also plays a role in determining the preferred spin ordering of the condensate. The quadratic Zeeman energy q can be controlled using the magnetic bias field; it can also be varied by using microwave dressing (e.g., see [30,31]).

B. Nematic order

To quantify the spin order it is useful to introduce the Cartesian representation of the spinor field $\vec{\psi} \equiv (\psi_x,\psi_y,\psi_z)$, where $\psi_x = (\psi_{-1}-\psi_1)/\sqrt{2}$, $\psi_y = -i(\psi_1+\psi_{-1})/\sqrt{2}$, and $\psi_z = \psi_0$. We give results in both the Cartesian $\vec{\psi}$ and the spherical [$\boldsymbol{\psi}$, see Eq. (1)] bases as needed.

A general spinor can be decomposed in the form

$$\vec{\psi} = e^{i\theta}(\vec{u} + i\vec{v}), \tag{4}$$

where θ is the global phase, $\{\vec{u},\vec{v}\}$ are mutually orthogonal real vectors satisfying $|\vec{u}|^2 + |\vec{v}|^2 = n$, and $|\vec{u}| \geqslant |\vec{v}|$ (also see [3,5,32,33]). For a spin-1 spinor, the local spin information described by the spin density vector is

$$\mathbf{F} = -i\vec{\psi}^* \times \vec{\psi} = 2\vec{u} \times \vec{v}, \tag{5}$$

and the symmetric nematic (or quadrupolar) tensor density is

$$\mathcal{N}_{ab} = \tfrac{1}{2}\langle f_a f_b + f_b f_a\rangle, \quad a,b \in \{x,y,z\} \tag{6}$$

$$= n\delta_{ab} - \tfrac{1}{2}(\vec{\psi}^* \otimes \vec{\psi} + \vec{\psi} \otimes \vec{\psi}^*) \tag{7}$$

$$= n\delta_{ab} - (\vec{u} \otimes \vec{u} + \vec{v} \otimes \vec{v}). \tag{8}$$

The nematic tensor describes the anisotropy of the spin fluctuations and, in general, has the symmetries of an ellipsoid. This is revealed by diagonalizing $\mathcal{N}$, giving $\{\vec{u},\vec{v},\mathbf{F}\}$ as the eigenvectors with respective eigenvalues $\lambda_u = \frac{1}{2}(n-\mathcal{A})$, $\lambda_v = \frac{1}{2}(n+\mathcal{A})$, and $\lambda_F = n$. Here $\mathcal{A} = 2|\vec{u}|^2 - n \geqslant 0$ is the *alignment parameter* [5], which characterizes the relative fluctuations of magnetization along the directions orthogonal to $\mathbf{F}$. The alignment is related to the spin-singlet amplitude [34],

$$\alpha = \vec{\psi}\cdot\vec{\psi} = \psi_0^2 - 2\psi_1\psi_{-1}, \tag{9}$$

as $\mathcal{A} = |\alpha|$. It is conventional to take the eigenvector associated with the smallest eigenvalue of $\mathcal{N}$ as the nematic director, i.e., the vector $\vec{u}$. We can use the eigenvectors and eigenvalues to represent the nematic tensor density as an ellipsoid [see Fig. 1(a)]. We also note that $\lambda_u = |\vec{v}|^2$ and $\lambda_v = |\vec{u}|^2$, so that the extent of the ellipsoid along the $\vec{u}$

direction is the squared length of $\vec{v}$, and the extent of the ellipsoid along the $\vec{v}$ direction is the squared length of $\vec{u}$.

Two limiting states are of interest. First, the fully magnetized ferromagnetic state with $|\mathbf{F}| = n$, where $|\vec{u}| = |\vec{v}| = \sqrt{n/2}$, and $\mathcal{A} = 0$. Second, and of primary concern in our work, is the fully polar (or spin-nematic) state, which has the form

$$\vec{\psi}_{\mathrm{P}} = e^{i\theta}\vec{u}, \tag{10}$$

with $|\vec{u}| = \sqrt{n}$, $\mathcal{A} = n$, and $\mathbf{F} = 0$ [see Figs. 1(b) and 1(c)]. The spin properties of this state are completely characterized by the director $\vec{u}$, and the state is invariant under the transformation

$$\theta \to \theta + \pi \quad \text{and} \quad \vec{u} \to -\vec{u}. \tag{11}$$

For general spin-1 states the relation

$$|\mathbf{F}|^2 + \mathcal{A}^2 = n^2 \tag{12}$$

holds, so that $\mathcal{A}$ can be used to characterize how close a state is to the limiting case of ferromagnetic ($\mathcal{A} = 0$) or polar ($\mathcal{A} = n$) order.

C. Order parameter for the EA-to-EP phase transition

Here we are concerned with an anti-ferromagnetic condensate in which a quench is performed by a sudden change in the quadratic Zeeman energy from a positive value to a negative value [35] crossing a quantum phase transition between two different ground states [see Fig. 1(d)]. In both cases the ground state is fully polar $\vec{\psi} = e^{i\theta}\vec{u}$. For $q > 0$ the director ($\vec{u}$) is along the z axis [EA phase; see Fig. 1(c)]. For $q < 0$ the director lies in the xy plane [EP phase; see Fig. 1(b)]. Thus the EP phase breaks the axial symmetry (invariance to spin rotations about z) of the Hamiltonian. This type of quench in an antiferromagnetic spinor condensate of ^{23}Na atoms has been performed in a number of experiments [17,18,20,21,36], however, the EP nematic order was not directly probed in these studies (cf. [5]). We also note that other phase transitions can be considered in this system, e.g., Witkowska *et al.* [37] considered a q quench for an antiferromagnetic condensate with a nonzero (conserved) z magnetization, where a transition to a phase-separated state occurs.

We would like to obtain an order parameter that can distinguish between these two states, notably the order parameter should be 0 in the EA phase and nonzero in the EP phase. To do this we note that in the EA phase the nematic tensor is isotropic in the xy plane [see Fig. 1(c)], while in the EP phase the nematic tensor is anisotropic in the xy plane [see Fig. 1(b)]. To quantify the EP nematic order, and taking motivation from nematic liquid crystals [38], we use a traceless symmetric tensor to quantify order in this system. Particular to the EA-to-EP phase transition we use the planar tensor,

$$Q = \mathcal{N}_{2\times 2} - \tfrac{1}{2}\mathrm{Tr}\{\mathcal{N}_{2\times 2}\}I_2 \tag{13}$$

$$= \begin{pmatrix} Q_{xx} & Q_{xy} \\ Q_{xy} & -Q_{xx} \end{pmatrix}, \tag{14}$$

where $\mathcal{N}_{2\times 2}$ is the xy submatrix of $\mathcal{N}$, and I_2 is the identity matrix. Evaluating this expression we find that $Q_{xx} = \mathrm{Re}\{\psi_1^*\psi_{-1}\}$ and $Q_{xy} = \mathrm{Im}\{\psi_1^*\psi_{-1}\}$, i.e., it depends on the relative phase coherence between the ψ_1 and the ψ_{-1} components of the system. While Q is traceless by construction, $\mathrm{Tr}(Q^2) = 0$ only when the spin fluctuations are isotropic in the xy plane. The EP phase is thus revealed by $\mathrm{Tr}(Q^2)$'s becoming nonzero, thus demonstrating how Q serves as an order parameter. We can write the eigenvalues of Q as $\{-\frac{1}{2}\mathcal{A}_\perp, \frac{1}{2}\mathcal{A}_\perp\}$, where we have defined a "transverse alignment" parameter [39],

$$\mathcal{A}_\perp = |\alpha_\perp|, \tag{15}$$

and have introduced [cf. Eq. (9)]

$$\alpha_\perp \equiv -2\psi_1\psi_{-1}. \tag{16}$$

Using this result gives $\mathrm{Tr}(Q^2) = \frac{1}{2}\mathcal{A}_\perp^2$. In Appendix A we present an alternative formulation of the planar tensor Q and order parameter results.

III. RESULTS

A. Quasi-two-dimensional quench

In order to explore the quench dynamics we focus on a quasi-2D system. In this regime the extent of the condensate in one direction (which we take to be z) is less than the spin healing length, so spin motion is effectively frozen out in this direction. This regime has been realized in experiments by applying a tight optical trap in this direction (e.g., see [23,40]). Additionally, we neglect any transverse confinement and take the condensate to be homogeneous in the plane. The dynamics of this system is described by the spin-1 Gross-Pitaevskii equation (GPE):

$$i\hbar\frac{\partial \boldsymbol{\psi}}{\partial t} = \left(-\frac{\hbar^2\nabla^2}{2M} + qf_z^2 + g_n n + g_s \boldsymbol{F}\cdot\boldsymbol{f}\right)\boldsymbol{\psi}. \tag{17}$$

Note that we have neglected the linear Zeeman shift, which can be removed from the equation of motion by transforming to a rotating frame.

To numerically solve this equation we represent each component of the spinor field $\boldsymbol{\psi}$ in a 2D square region of dimensions $l \times l$ covered by an $N \times N$ grid of equally spaced points. Taking periodic boundary conditions for the solution we evaluate spatial derivatives in the kinetic energy term of Eq. (17) with spectral accuracy using fast Fourier transforms. To evolve the GPE in time we use the second-order symplectic method presented in Ref. [41].

The initial condition for the simulations is a uniform EA ground state (in the spherical basis),

$$\boldsymbol{\psi}(\mathbf{x}, t = 0) = \sqrt{n_c}\begin{pmatrix} 0 \\ 1 \\ 0 \end{pmatrix} + \boldsymbol{\delta}(\mathbf{x}), \tag{18}$$

where n_c is the condensate (areal) density and $\boldsymbol{\delta}$ is a small noise field added to seed the growth of unstable modes following the quench. The late-time results are insensitive to the form of white spatial noise we add to the initial state as long as the noise is weak ($|\boldsymbol{\delta}|^2 \ll n_c$). We choose to add noise according to the truncated Wigner prescription [42], which is consistent with the quantum vacuum noise in the initial state (see [43] for details). We introduce the characteristic spin energy

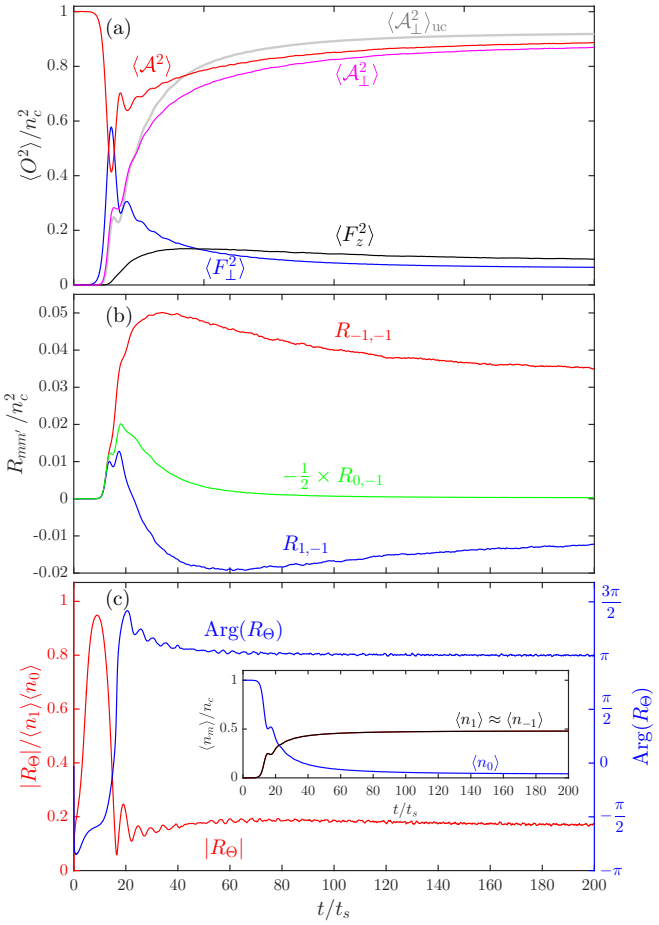

FIG. 2. Growth of densities, local pair correlations, and R_Θ following a quench from the EA to the EP phase. (a) The local densities $O = \{n, \mathcal{A}, \mathcal{A}_\perp, \mathbf{F}\}$ are evaluated from the results of a single simulation trajectory according to Eq. (19). (b) Local pair correlations functions, as defined in Eq. (20). (c) Relative phase correlation function R_Θ as defined in Eq. (22). Inset: Evolutions of the mean component densities, noting that the $m = \pm 1$ results are approximately identical. Simulation is for a quench to $q = -0.5 q_0$ with $g_n = 3 g_s$. The simulation is for a condensate density $n_c = 10^4/\xi_s^2$ of size $l = 400\,\xi_s$ with $N = 512$ points in each direction.

$q_0 \equiv 2 g_s n_c$ and associated spin healing length $\xi_s = \hbar/\sqrt{M q_0}$ and spin time $t_s = \hbar/q_0$ as convenient units.

B. Early-time dynamics: Development of local order

Immediately following the quench the initial EA state is unstable and begins to evolve towards the new phase. Aspects of these early-time dynamics and the emergence of local EP order can be revealed by studying the behavior of the spin and alignment densities. Since some of these densities (e.g., F_z) can be locally negative, we quantify the development of a particular density of interest O by spatially averaging O^2, i.e., we evaluate

$$\langle O^2(t) \rangle = \frac{1}{l^2} \int d^2\mathbf{x}\, O^2(\mathbf{x}, t). \tag{19}$$

We present results for a variety of densities of interest in Fig. 2(a). These results show that immediately following the quench the EA state becomes dynamically unstable to magnon excitations, which grow exponentially and cause the system to develop transverse magnetization [i.e., $\mathbf{F}_\perp = (F_x, F_y)$]. The precise nature of the instability and the wave vectors of the unstable modes depends upon the value of q, and aspects of this have been explored in experiments [17,18,21,36]. The axial magnetization (F_z) similarly experiences exponential growth. The general behavior of spin density growth we observe is similar for quenched condensates with ferromagnetic interactions (e.g., see [31,44–46]). Noting that the average z magnetization of the initial state is 0 (and conserved), the quantity $\langle F_z^2(t) \rangle$ corresponds to the fluctuations in magnetization studied in recent experiments [36].

More direct insight into the change in nematic order is provided by the alignment densities $\{\mathcal{A}, \mathcal{A}_\perp\}$ discussed in Sec. II B. The initial EA state is fully aligned (i.e., $\mathcal{A} = n_c$), but this dips down in the early dynamics as the magnetization develops [as required by relation (12)]. As the alignment is restored for $t \gtrsim 20 t_s$ it is of a different character, consistent with EP order emerging. We see this by evaluating the transverse alignment $\mathcal{A}_\perp$ order, which is initially negligible but then grows and is seen to saturate towards the value of $\mathcal{A}$.

Various *in situ* measurements of correlations between components of the density have been performed in spinor condensate experiments (e.g., see [18,24,36,47]). Most relevant to our system are the measurements by Vinit *et al.* [18] of the time evolution of the local pair correlation function following the EA-to-EP quench of a quasi-one-dimensional antiferromagnetic condensate. The correlation functions measured were [48]

$$R_{mm'}(t) = \langle \delta n_m \delta n_{m'} \rangle, \tag{20}$$

where $\delta n_m(\mathbf{x}, t) = n_m(\mathbf{x}, t) - \langle n_m \rangle$ is the m-component density fluctuation operator, with $n_m = |\psi_m|^2$ and $\langle n_m \rangle$ being the mean density of this component. We have evaluated the same correlation functions measured in experiments (cf. Fig. 3 in Ref. [18]) and present the results in Fig. 2(b). We find qualitative behavior similar to their results, however, note that their measurements were for a shallow quench (to $q \approx -0.02 q_0$) and with appreciable thermal effects. These same types of local density measurements could be used to evaluate the alignment densities. Indeed, noting that $\langle \mathcal{A}_\perp^2 \rangle = 4 \langle n_1 n_{-1} \rangle$ [see Eqs. (15) and (16)], taking n_1 and n_{-1} as uncorrelated, we can make the estimate

$$\langle \mathcal{A}_\perp^2 \rangle_{\rm uc} \approx 4 \langle n_1 \rangle \langle n_{-1} \rangle. \tag{21}$$

For the uniform system $\langle n_m \rangle = N_m/l^2$, and thus $\langle \mathcal{A}_\perp^2 \rangle_{\rm uc}$ is determined by the component populations $N_m = \int d^2\mathbf{x} n_m$, which are readily measured in experiments. As shown in Fig. 2(a) the uncorrelated approximation tends to overestimate the EP order ($\langle \mathcal{A}_\perp^2 \rangle$) once it develops ($t \gtrsim 20 t_s$). Noting that $\langle n_1 n_{-1} \rangle = \langle n_1 \rangle \langle n_{-1} \rangle + R_{1,-1}$, this overestimate of Eq. (21) is due to the negative value $R_{1,-1}$ takes for $t \gtrsim 20 t_s$ [Fig. 2(b)]. Evidence of $R_{1,-1}$'s becoming negative was also found in experiments at late times [18].

Finally, we examine the system evolution to quantify the local "phase locking" of the $m = \pm 1$ components relative to the $m = 0$ component. This was recently observed in experiments by applying a spin rotation to the system and

measuring the resulting magnetic fluctuations [5]. In our simulations we can directly access this from the local (spatially averaged) correlation function

$$R_\Theta(t) \equiv \langle \psi_{-1}\psi_1\psi_0^*\psi_0^* \rangle. \tag{22}$$

Taking $\psi_m = \sqrt{n_m}e^{i\theta_m}$, we see that $R_\Theta \sim e^{i(\theta_1+\theta_{-1}-2\theta_0)}$, which conventionally defines the relative phase $\Theta \equiv \theta_1 + \theta_{-1} - 2\theta_0$. To understand the physical relevance of this correlation function, we note that the transverse spin density squared and the alignment density squared are

$$\langle |F_\perp|^2 \rangle = 2\langle n_0(n_{-1}+n_1)\rangle + 4\mathrm{Re}\{R_\Theta\}, \tag{23}$$

$$\langle \mathcal{A}^2 \rangle = \langle n_0^2 \rangle + 4\langle n_1 n_{-1}\rangle - 4\mathrm{Re}\{R_\Theta\}, \tag{24}$$

respectively. Thus varying the real part of R_Θ enables the system to enhance or reduce the spin density, while having the opposite effect on the alignment [also see Eq. (12)]. Antiferromagnetic systems prefer $\Theta = \pi$ to reduce the spin density. The behavior of R_Θ is shown in Fig. 2(c); note that we have normalized R_Θ by the average densities of each component [using $\langle n_{-1}\rangle \approx \langle n_1\rangle$; also see inset in Fig. 2(c)] so that the magnitude measures the concentration of Θ. These results show that after the early dynamics settles down ($t \gtrsim 25t_s$) the function R_Θ approaches a negative real value, i.e., $\Theta \to \pi$. The $m = 0$ component is unoccupied in the EP ground state but maintains a small population [see inset in Fig. 2(c)] at late times due to heating from the quench. The $m = 0$ component of the system is noisy (consistent with a thermalized gas, e.g., see [43]) and the amplitude of the R_Θ correlation function is significantly reduced by these fluctuations. However, our results show that there is still a tendency for the spin-dependent interactions to lock the relative phase of the $m = \pm 1$ components relative to the $m = 0$ component.

C. Late-time universal coarsening dynamics

In addition to considering the emergence of local spin-nematic order we wish to examine the spatial dependence of the textures (domains) that develop and how these evolve in time. In Fig. 3 we visualize the system order in a region of a simulation soon after local order is established [Fig. 3(a)] and at a later time [Fig. 3(b)]. This visualization is performed by decomposing the spinor field at each simulation point according to Eq. (4) to obtain $\vec{u}(\mathbf{x})$ and $\theta(\mathbf{x})$. The results in Fig. 3 demonstrate that the spin-nematic and superfluid (i.e., global phase θ) order tends to extend over larger length scales as time passes, showing that the system is coarsening toward an EP state with (quasi-)long-range order.

To quantify the spatial dependence of the ordering we introduce the correlation functions

$$G_\phi(\mathbf{r},t) = \frac{2}{n_c^2}\langle \mathrm{Tr}\{Q(\mathbf{0})Q(\mathbf{r})\}\rangle_t, \tag{25}$$

$$G_\theta(\mathbf{r},t) = \frac{1}{n_c^2}\langle \alpha_\perp^*(\mathbf{0})\alpha_\perp(\mathbf{r})\rangle_t \tag{26}$$

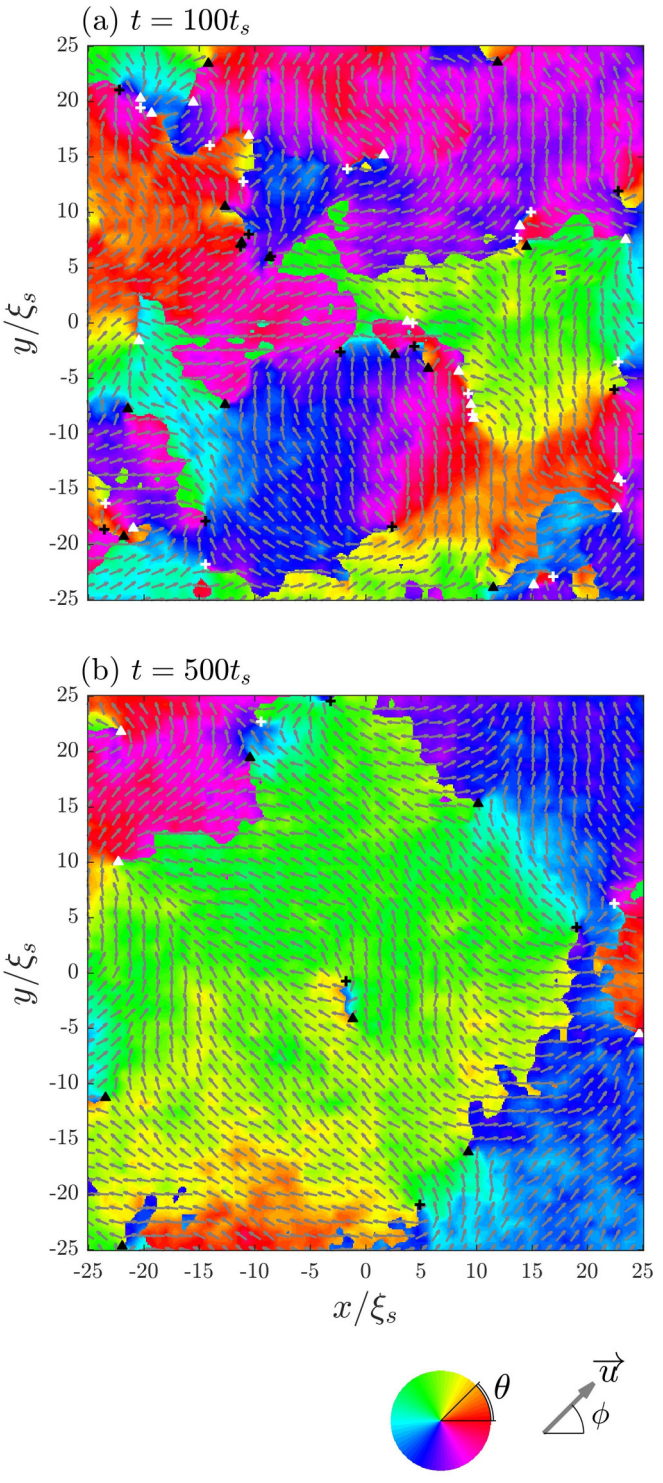

FIG. 3. Evolution of order after the quench in a $50\xi_s \times 50\xi_s$ subregion of a simulation at (a) $t = 100t_s$ and (b) $t = 500t_s$. Arrows indicate planar projection of the director $\vec{u}$ and colors indicate the phase order θ in these regions. In general there are two possible values, $\vec{u}$ and θ, for the spinor at each simulation point [see Eq. (4)] because of the symmetry, (11), and we impose the further condition $u_y \geqslant 0$. We also show the locations of HQVs (see Sec. III D) with circulations $\sigma_1 = 1$ (black cross), $\sigma_1 = -1$ (black triangle), $\sigma_{-1} = 1$ (white cross), and $\sigma_{-1} = -1$ (white triangle). Simulation parameters: $g_n = 3g_s$, $q = -0.5\,q_0$, $n_c = 10^4/\xi_s^2$, $l = 200\,\xi_s$, and $N = 256$ points.

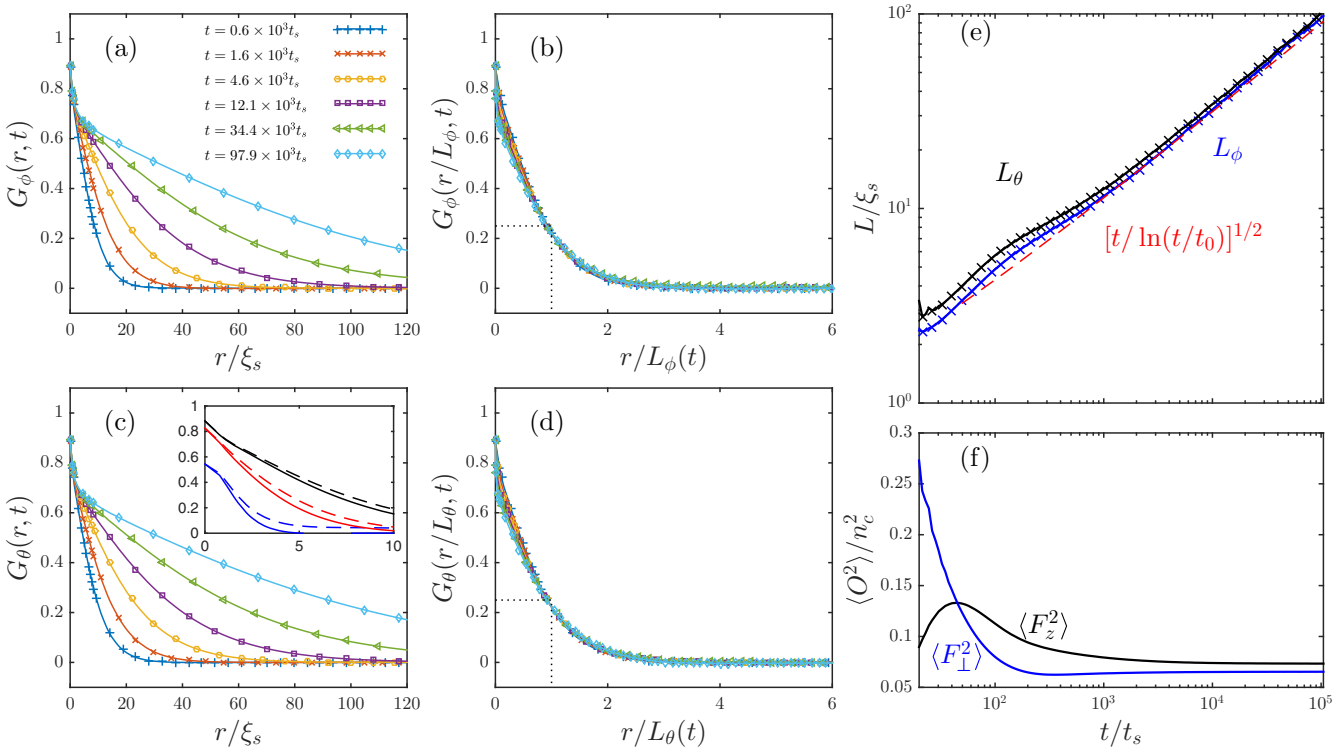

FIG. 4. Evolution and dynamic scaling of order parameter correlation functions. (a) Spin-nematic order correlation function G_ϕ at various times after the quench. (b) Collapse of the G_ϕ correlation functions when space is scaled by the length scale $L_\phi(t)$. (c) Superfluid order correlation function G_θ at various times after the quench. Inset: Comparison of G_ϕ (solid lines) and G_θ (dashed lines) at $t/t_s = 25.6$ (blue lines), 99.0 (red lines), and 399 (black lines). (d) Collapse of the G_θ correlation functions when space is scaled by the length scale $L_\theta(t)$. (e) Evolution of the length scales L_ϕ and L_θ compared to a $[t/\ln(t/t_0)]^{1/2}$ growth law, where $t_0 = 0.5t_s$. (f) Evolution of magnetic fluctuations. Simulations are performed on a domain of size $l = 1600\xi_s$ covered by $N = 2048$ points and averaged over 15 trajectories. Interactions are $g_n = 3g_s$, $n_c = 10^4/\xi_s^2$, and $q = -0.5\,q_0$.

for the spin-nematic and superfluid orders, respectively, evaluated at time t after the quench. See Appendix B for more details about how these correlation functions relate to the atomic-field operators.

To illustrate the use of these correlation functions, we consider the EP ground-state spinor

$$\boldsymbol{\psi}_{\rm EP} = \sqrt{\frac{n_c}{2}} e^{i\theta} \begin{pmatrix} -e^{-i\phi} \\ 0 \\ e^{i\phi} \end{pmatrix}, \tag{27}$$

where the angle ϕ is associated with the spin-nematic order (i.e., $\vec{u} \propto \cos\phi\,\hat{\mathbf{x}} + \sin\phi\,\hat{\mathbf{y}}$) and the global phase θ is associated with the superfluid order. Taking θ and ϕ to be spatially dependent random variables, we use $\boldsymbol{\psi}_{\rm EP}$ to evaluate the correlation functions (25) and (26), yielding

$$G_\phi^{\rm EP}(\mathbf{r}) = \langle \cos 2[\phi(\mathbf{r}) - \phi(\mathbf{0})] \rangle, \tag{28}$$

$$G_\theta^{\rm EP}(\mathbf{r}) = \left\langle e^{i2[\theta(\mathbf{r}) - \theta(\mathbf{0})]} \right\rangle. \tag{29}$$

In practice we compute the spin-nematic order parameter correlation function as

$$G_\phi(r,t) = \int d\Omega_r \int \frac{d^2\mathbf{x}'}{l^2} \frac{2}{n_c^2} \langle {\rm Tr}\{Q(\mathbf{x}')Q(\mathbf{x}'+\mathbf{r})\} \rangle_t, \tag{30}$$

which includes averaging to improve the statistics of our results: $\langle\,\rangle_t$ denotes an average over trajectories (simulations with different seeding noise). The integral $\int d\Omega_r$ is an angular average in 2D position space (utilizing the isotropy of the system) and $l^{-2}\int d^2\mathbf{x}'$ denotes spatial averaging. The convolutions are efficiently computed using fast Fourier transforms. We also apply these additional averaging steps when computing the $G_\theta(r,t)$ correlation function.

Results for the evolution of $G_\phi(r,t)$ are shown in Fig. 4(a). As time increases the correlation function is seen to decay more slowly, indicating that the in-plane spin-nematic order is extending over larger distances. We can investigate whether the growth of this order exhibits dynamic scaling whereby the nematic domains are statistically self-similar at different times, up to an overall length scale that grows with time. This property often holds in the late-time (when the domain sizes are much larger than the microscopic length scales of the system) phase-ordering dynamics of systems [49]. To verify dynamic scaling we demonstrate that the correlation function collapses to a universal (time-independent) function under time-dependent rescaling of space, i.e., by showing that with an appropriate choice of $L_\phi(t)$ we have

$$H_\phi(r) = G_\phi(r/L_\phi(t),t). \tag{31}$$

Results showing the collapse are presented in Fig. 4(b), where we have taken $L_\phi(t)$ to be the correlation length defined by the distance over which the correlation function decays to one-fourth of its local value, i.e., $G_\phi(L_\phi,t) = \frac{1}{4}G_\phi(0,t)$. The

collapse is reasonably good except at short length scales ($r \ll L_\phi$), where the correlation function sharpens as t increases.

The length scale $L_\phi(t)$ is not unique and can be multiplied by a constant and still yield correlation function collapse. However, as chosen $L_\phi(t)$ gives a reasonable characterization of the domain size [50] in the ordering EP system. By considering the evolution of $L_\phi(t)$ we can extract the dynamic critical exponent z_ϕ as $L_\phi(t) \sim t^{1/z_\phi}$, providing a key characterization of the dynamic universality class of the system. In Fig. 4(e) we show the time evolution of $L_\phi(t)$ in a log-log graph and find that at late times ($t \gtrsim 10^3 t_s$) this grows as $L_\phi(t) \sim [t/\ln(t/t_0)]^{1/2}$, i.e., with a dynamic critical exponent of $z_\phi = 2$ and logarithmic corrections. We find that the growth law exhibits a slight bulge (i.e., above the asymptotic growth law) extending from early times up until times of order $10^3 t_s$. We find that this correlates with the time period over which the magnetic fluctuations evolve appreciably in the system [see Fig. 4(f)], suggesting that the decay of magnetic fluctuations may set an important time scale for the system entering into the late-time coarsening regime (also see [36]).

The $L_\phi(t) \sim [t/\ln(t/t_0)]^{1/2}$ growth law we obtain here is the same form of growth known from the dissipative 2D XY model [51,52] (also see [53]) and was established in early work considering the coarsening dynamics of smectic liquid crystal films [54] (also see [55–57]). Singh *et al.* [56] have predicted an analytic form of H_ϕ for nematic liquid crystals, which they have favorably compared to the results of Monte Carlo simulations using a spin-nematic liquid crystal model [11]. We, however, find that this result is not a good fit to the H_ϕ we obtain.

We can also consider the superfluid scaling in this system, with examples of the evolving G_θ correlation function shown in Fig. 4(c). We verify dynamic scaling in a similar way to the spin-nematic order by finding a length scale $L_\theta(t)$ such that we have correlation function collapse:

$$H_\theta(r) = G_\theta(r/L_\theta(t),t). \tag{32}$$

Results showing this collapse are presented in Fig. 4(d), where again we have taken $L_\theta(t)$ to be the distance over which the correlation function decays to one-fourth of its local value. These results also reveal that the late-time superfluid correlation function G_θ has a shape similar to that of the spin-nematic correlation function G_ϕ. By definition both correlation functions have the same local value, i.e., $G_\theta(0) = G_\phi(0) = \langle \mathcal{A}_\perp^2 \rangle / n_c^2$. However, in general the superfluid correlation function decays more slowly and has a slightly longer characteristic length than the spin-nematic correlation function [e.g., see inset in Fig. 4(c)].

In Fig. 4(e) note that L_θ grows in a similar way to L_ϕ, consistent with the same dynamical critical exponent, i.e., $z_\theta \approx z_\phi \approx 2$ (to within log corrections). Thus we find that the superfluid and spin-nematic order grow together in this system. This is different from recent results for the ordering of an EA ferromagnetic phase of a spin-1 condensate, which showed that the superfluid order grows significantly more slowly than the spin order [22] (also see [58]). We also note that Ref. [22] demonstrates how the late-time coarsening results are insensitive to the resolution of the numerical grid used in simulations. Our particular choice of grid-point spacing $\Delta x = l/N = 0.78\,\xi_s$ is to resolve the unstable modes that dominate the early-time dynamics following the quench.

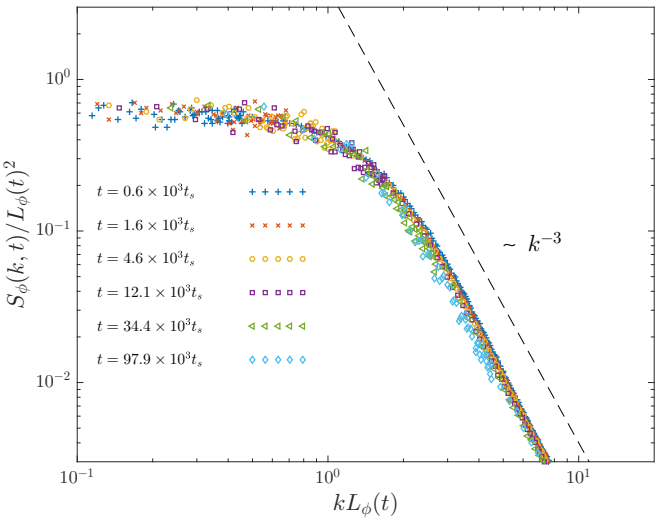

FIG. 5. S_ϕ structure factor scaled by $L_\phi(t)$ to reveal the scaling collapse. The power-law decay for $kL_\phi > 1$ reveals the Porod tail, with a guide line indicating k^{-3} scaling for reference. Other parameters as in Fig. 4.

It is conventional also to analyze the structure factors associated with the order parameter correlation function. The structure factor for spin-nematic order is defined as

$$S_\phi(\mathbf{k},t) = \int d^2\mathbf{r}\, G_\phi(\mathbf{r},t) e^{i\mathbf{k}\cdot\mathbf{r}}. \tag{33}$$

The structure factors also collapse with dynamic scaling according to

$$S_\phi(\mathbf{k},t) = L_\phi(t)^2 \hat{h}\big(\mathbf{k}L_\phi(t)\big), \tag{34}$$

where $\hat{h}$ is the Fourier transform of H_ϕ, (31). Results for the S_ϕ structure factor are shown in Fig. 5. For k vectors in the range $L_\phi^{-1} < k \ll \xi_s^{-1}$ (i.e., length scales between the microscopic healing length and the domain size), the structure factor exhibits a power-law decay that is approximately of the form k^{-3}. This differs from the generalized Porod law result of k^{-4} decay expected in 2D spin models [57,59]. The k^{-3} decay law is also found for the first-order structure factors (single-particle momentum spectra) in studies of binary condensates in relevant regimes [29] and is analyzed in terms of turbulence scaling.

We can similarly define a superfluid structure factor S_θ from G_θ. This structure factor has a collapse and power-law decay similar to those we have presented for $S_\phi(k)$.

D. Topological defects

It is of interest to consider HQVs, which are the topological defects supported by the EP order parameter. To illustrate the properties of HQVs we first consider a single HQV located at the origin. Away from the core the wave function is approximately of the form

$$\boldsymbol{\psi}_{\rm vort} = \sqrt{\frac{n_c}{2}} e^{iq_\theta\varphi} \begin{pmatrix} -e^{-iq_\phi\varphi} \\ 0 \\ e^{iq_\phi\varphi} \end{pmatrix} \sim \begin{pmatrix} -e^{-i\sigma_1\varphi} \\ 0 \\ e^{i\sigma_{-1}\varphi} \end{pmatrix}, \tag{35}$$

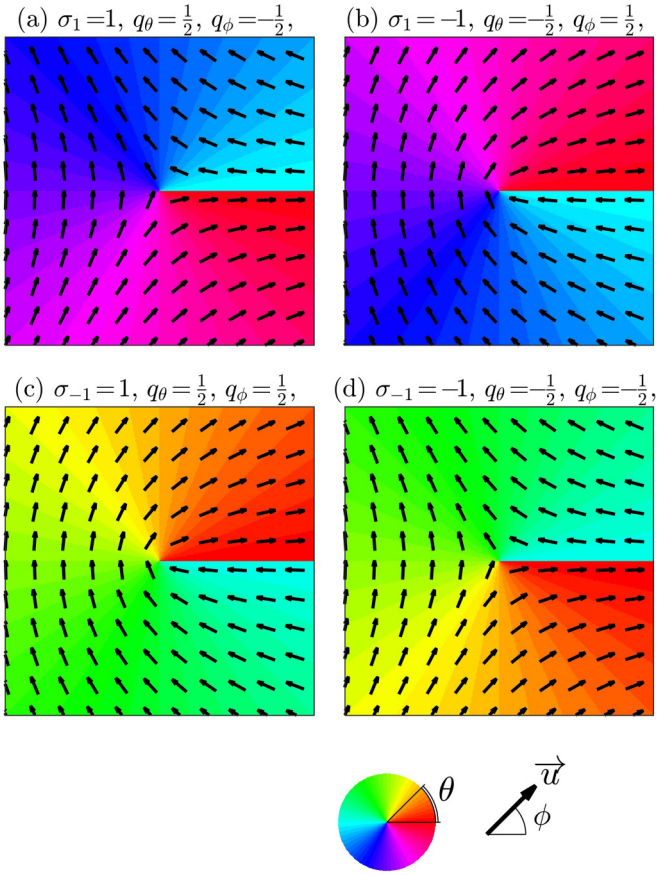

FIG. 6. (a–d) Four types of HQVs that can occur in the EP phase are illustrated, labeled by their winding numbers.

where we have set $\theta \to q_\theta\varphi$ and $\phi \to q_\phi\varphi$ in Eq. (27), φ is the azimuthal angle about the core, and $\{q_\theta, q_\phi\}$ are the winding numbers. In Eq. (35) we have also introduced the component windings

$$\sigma_{\pm 1} \equiv q_\theta \mp q_\phi, \tag{36}$$

where σ_m denotes the net phase winding in the mth component of the field. The σ_m must be integers for the field to be single-valued. The cases $\sigma_1 = \pm 1$ (with $\sigma_{-1} = 0$) and $\sigma_{-1} = \pm 1$ (with $\sigma_1 = 0$) define the four HQVs, corresponding to $q_\theta = \pm\frac{1}{2}$, $q_\phi = \pm\frac{1}{2}$, i.e., vortices with half-quantized values of the windings in θ and ϕ (see Fig. 6).

Much of our theoretical understanding of HQV dynamics has come from studies of miscible two-component condensates [60–62], which also support HQVs (also see [63]). Notably, Eto *et al.*, [61] have shown that the interaction potential between two HQVs separated by a distance R (for $R \gg \xi_s$) is of the form

$$U_{\rm int} \propto \kappa \ln R, \tag{37}$$

where

$$\kappa = q_\theta^{(1)} q_\theta^{(2)} + q_\phi^{(1)} q_\phi^{(2)} = \frac{1}{2} \sum_{m=\pm 1} \delta_{\sigma_m^{(1)},\sigma_m^{(2)}}, \tag{38}$$

with $(q_\theta^{(1)}, q_\phi^{(1)})$ and $(q_\theta^{(2)}, q_\phi^{(2)})$ [or $(\sigma_1^{(1)}, \sigma_{-1}^{(1)})$ and $(\sigma_1^{(2)}, \sigma_{-1}^{(2)})$] being the sets of winding numbers specifying HQV 1 and HQV 2, respectively. In the case where both HQVs have winding in the same component (i.e., both having $|\sigma_1| = 1$ or $|\sigma_{-1}| = 1$), then $|\kappa| = \frac{1}{2}$ and the interaction is of the same form as that for U(1) vortices in a scalar condensate. When the vortices occur in different components, then $\kappa = 0$ and there is no long-ranged interaction. However, a short-ranged repulsive interaction is predicted, extending over a length scale comparable to the vortex core size [61,63,64]. Two HQVs with opposite circulation in the same component (e.g., an HQV with $\sigma_1 = 1$ and an HQV with $\sigma_1 = -1$) can collide and annihilate, as has recently been observed in experiments [24].

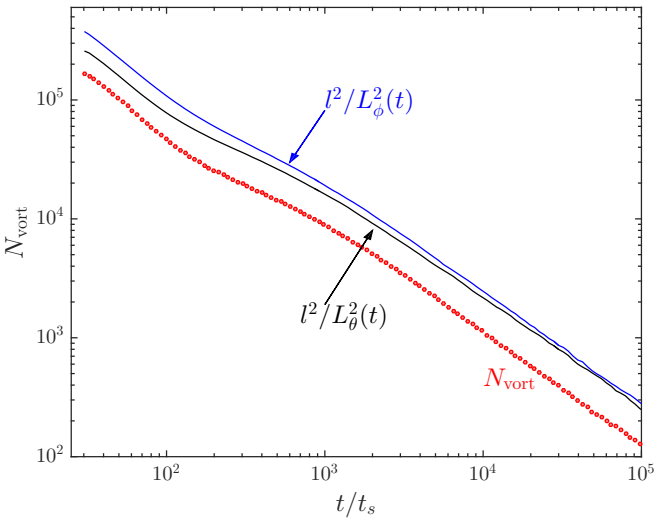

FIG. 7. HQV number as a function of time for the simulation case examined in Fig. 4. The vortex number is computed as the total number of unit phase winding singularities in the $m = \pm 1$ components averaged over the trajectories. The vortex number is compared to the *number of domains* l^2/L_v^2, using the characteristic length scales $L_v = \{L_\phi, L_\theta\}$ [from Fig. 4(e)] as labeled in the plot.

Coarsening dynamics can be viewed in terms of the dynamics of topological defects of the order parameter which are generated in the early stages of the quench dynamics. The windings associated with these defects disrupt the order, and as they mutually annihilate, order is able to extend over larger length scales. We show the locations of HQVs in Fig. 3, which reveals a qualitative relationship between the domain sizes and the vortex locations. To quantify the role of defects we detect the number of vortices in our simulations during the evolution. In practice we identify vortices by detecting integer phase windings of the field that occur around plaquettes of the numerical grid. If such phase windings occur only in the $m = 1$ or $m = -1$ component of the field and are spatially isolated from other vortices, then they can be identified as one of the four types of HQVs. Furthermore, HQVs have a z-magnetized core, which we observe in our simulations. In the early-time dynamics not all vortices detected are HQVs, but we find that only HQVs persist at late times ($t \gtrsim 100 t_s$). In Fig. 7 we show the averaged total number of vortices $N_{\rm vort}$ as a function of the time. The number of vortices decreases as the coarsening progresses. We can compare these results to the characteristic length scales discussed in Sec. III C. Crudely, if the characteristic length scale is taken to be the distance

between vortices, then we would expect

$$N_{\rm vort}(t) \sim \frac{l^2}{L_\nu(t)^2}, \quad \nu \in \{\phi,\theta\}. \tag{39}$$

We have added these results for the characteristic length to Fig. 7, verifying that relationship (39) holds.

As noted above a pair of $\sigma_1 = 1$ and $\sigma_1 = -1$ HQVs (or a $\sigma_{-1} = 1$ and $\sigma_{-1} = -1$ pair) evolves similarly to a vortex-antivortex pair in a scalar condensate and has the potential to mutually annihilate. In this case each component vortex experiences a Magnus force which causes the pair to move at a uniform velocity in a direction perpendicular to the line joining them. Such motion, without some other source of dissipation, does not lead to the vortices' meeting and annihilating. This is in contrast to oppositely charged polar core spin vortices (the topological defects of the easy-plane ferromagnetic phase), which accelerate towards each other and annihilate [65,66]. We expect that in our system dissipation will arise from the interaction between the vortices and the sound waves (spin waves) excited by the quench. However, recent results on HQVs suggest an additional dissipative mechanism even in the absence of spin waves: GPE simulations of a quiet binary condensate (without excitation) showed that such a pair of HQVs moves together and annihilates (see Sec. IV in [62]). This effect was observed to be dependent on the interaction parameter regime, occurring only for $\gamma > 0.5$, where γ is the ratio of the interspecies to the intraspecies interaction in the binary condensate. In the spin-1 system [67] this parameter relates to the interaction parameters as $\gamma \approx (g_n - g_s)/(g_n + g_s)$. Since our main simulations presented are for $\gamma = 0.5$, where this additional dissipative effect is expected to be negligible, it is of interest to see if our coarsening dynamics changes for a larger value of γ. To explore this issue we have conducted quench simulations for $g_s = g_n/12$ ($\gamma \approx 0.85$). The results for these simulations are roughly comparable to our main results in Fig. 4 (which are for $g_s = g_n/3$) and do not indicate that the coarsening proceeds at a faster rate. Nevertheless, obtaining a better understanding of HQV dynamics, particularly in the spin-1 system at finite q values, would be a valuable direction for future research. Also, a more detailed study of the dynamics and correlations between HQVs during the coarsening will be needed to illuminate the microscopic processes that are important in the system evolution (cf. [68]).

IV. CONCLUSION

In this paper we have presented a theory for quantifying order formation in an antiferromagnetic spin-1 condensate. We have used this to study the dynamics of a quasi-2D system quenched into the EP spin-nematic phase. This topic has been of growing interest, with a number of experimental developments motivating this work. These include studies of correlations and spatial ordering in a quasi-one-dimensional system [17,18] and the evolution of magnetic fluctuations and HQV formation in a quasi-2D system [36]. A key issue has been identifying appropriate observables for quantification of spin-nematic order. This issue has been explored by Zibold *et al.* [5], who developed a novel measurement scheme to demonstrate spin-nematic order in the single-mode regime [5]. We motivate and define order parameters for the system to quantify the spin-nematic and superfluid order, and in doing this we have connected our formalism to quantities that have already been measured in experiments.

We have also studied the universal coarsening regime that emerges at late times after the quench. We evaluate the evolution of the order parameter correlation functions by averaging over an ensemble of large-scale numerical simulations and show that both types of order exhibit dynamic scaling, with a characteristic length scale that grows as $L \sim [t/\log(t/t_0)]^{1/2}$. Our results also show that the coarsening is determined by the mutual annihilation of HQVs produced in the early stages of the quench. In experiments it may be difficult to directly measure the order parameter correlation function, whereas the average distance between HQVs (which can be directly imaged [23,24,36]) will be a more convenient method to measure a characteristic length scale of order in the system. While the main coarsening results presented are for the numerically convenient case of $g_n/g_s = 3$, we have also conducted simulations for higher ratios (closer to the ratio of the experimentally relevant species ^{23}Na) and found that the scaling is unchanged, as expected for universal behavior.

Having developed and applied a formalism for nonferromagnetic ordering in a spin-1 system we open the door to other studies of ordering in spinor systems. This includes the rich array of spin orders that emerge in higher spin systems (e.g., see [4]) and systems with topological interfaces [69,70].

ACKNOWLEDGMENTS

The authors acknowledge support from the Marsden Fund of the Royal Society of New Zealand. P.B.B. thanks Y. Kawaguchi for feedback on an early draft of the formalism, acknowledges useful discussions with L. Williamson, and thanks B. T. Wong for support of this research.

APPENDIX A: PLANAR TREATMENT OF SPIN-NEMATIC ORDER

We can formulate our order parameters by considering the Cartesian spinor field projected onto the plane:

$$\vec{\psi}_\perp \equiv (\psi_x, \psi_y)^T. \tag{A1}$$

Recalling that $\psi_x = \frac{1}{\sqrt{2}}(\psi_{-1} - \psi_1)$, $\psi_y = -\frac{i}{\sqrt{2}}(\psi_1 + \psi_{-1})$, we see that the planar treatment depends only on the $\{\psi_1, \psi_{-1}\}$ spherical components of the spinor.

We now proceed to develop a mathematical description of the spin properties of the planar-spin system analogously to the three-dimensional treatment developed in Sec. II B. We can decompose the planar spinor into two real planar vectors,

$$\vec{\psi}_\perp = e^{i\theta_\perp}(\vec{u}_\perp + i\vec{v}_\perp), \tag{A2}$$

which are orthogonal and satisfy the normalization condition

$$|\vec{u}_\perp|^2 + |\vec{v}_\perp|^2 = n_\perp, \tag{A3}$$

where $n_\perp = \vec{\psi}_\perp^* \cdot \vec{\psi}_\perp = n_1 + n_{-1}$. We choose $\vec{u}_\perp$ to be the effective planar director and take it to be the longest vector, i.e., $|\vec{u}_\perp|^2 \geqslant \frac{1}{2}n_\perp \geqslant |\vec{v}_\perp|^2$. We emphasize that the vectors $\{\vec{u}_\perp, \vec{v}_\perp\}$ are not in general the projected versions of the three-dimensional vectors in Eq. (4) (e.g., projection of $\{\vec{u}, \vec{v}\}$ does not preserve their orthogonality).

Because our vectors are 2D we can only obtain a z component of the cross product, which yields the usual $F_z = |\psi_1|^2 - |\psi_{-1}|^2$ magnetization density, i.e.,

$$F_z = -i\vec{\psi}_\perp^* \times \vec{\psi}_\perp = 2\vec{u}_\perp \times \vec{v}_\perp. \tag{A4}$$

The $m = 0$ component projected out of the spinor prohibits us from quantifying the transverse magnetization. The singlet amplitude to the planar system is defined as

$$\alpha_\perp \equiv \vec{\psi}_\perp \cdot \vec{\psi}_\perp = -2\psi_1\psi_{-1} \tag{A5}$$

and we have the relation [cf. Eq. (12)]

$$F_z^2 + |\alpha_\perp|^2 = n_\perp^2. \tag{A6}$$

We can construct a symmetric traceless tensor [i.e., the one introduced in Eq. (13)] as

$$Q \equiv \frac{n_\perp}{2} I_2 - \frac{1}{2}(\vec{\psi}_\perp^* \otimes \vec{\psi}_\perp + \vec{\psi}_\perp \otimes \vec{\psi}_\perp^*) \tag{A7}$$

$$= \frac{n_\perp}{2} I_2 - (\vec{u}_\perp \otimes \vec{u}_\perp + \vec{v}_\perp \otimes \vec{v}_\perp). \tag{A8}$$

As noted in Sec. II C the elements of Q in spherical spinor components are $Q_{xx} = \mathrm{Re}\{\psi_1^*\psi_{-1}\} = -Q_{yy}$ and $Q_{xy} = \mathrm{Im}\{\psi_1^*\psi_{-1}\}$, with $\det(Q) = -n_1 n_{-1}$.

By inspection of Eq. (A8) we see that $\{\vec{u}_\perp, \vec{v}_\perp\}$ are eigenvectors of Q with eigenvalues $\lambda_u = \frac{1}{2}n_\perp - |\vec{u}_\perp|^2$ and $\lambda_v = \frac{1}{2}n_\perp - |\vec{v}_\perp|^2$, respectively. Given our convention of choosing $\vec{u}_\perp$ as the longer vector we have that λ_u is negative (i.e., the director corresponds to the lowest eigenvalue). Because the matrix is traceless the eigenvalues are given by $\pm\sqrt{-\det(Q)}$, i.e., $\lambda_u = -\sqrt{n_1 n_{-1}}$ and $\lambda_v = \sqrt{n_1 n_{-1}}$. The trace of Q^2 is then just the sum of the eigenvalues squared, and recalling the transverse alignment $\mathcal{A}_\perp = |\alpha_\perp| = \sqrt{2n_1 n_{-1}}$, we obtain

$$\mathrm{Tr}(Q^2) = \tfrac{1}{2}\mathcal{A}_\perp^2. \tag{A9}$$

We also note that Q can be written in the form

$$Q = \frac{\mathcal{A}_\perp}{2}\begin{pmatrix} \cos 2\varphi & \sin 2\varphi \\ \sin 2\varphi & -\cos 2\varphi \end{pmatrix}, \tag{A10}$$

where we have introduced $\varphi \equiv \frac{1}{2}\mathrm{Arg}(\psi_1^*\psi_{-1})$, i.e., $\psi_1^*\psi_{-1} = \frac{1}{2}\mathcal{A}_\perp e^{2i\varphi}$. Note that this has eigenvalues and eigenvectors

$$\lambda_u = -\frac{\mathcal{A}_\perp}{2}, \quad \hat{\vec{u}}_\perp = \begin{pmatrix} \cos\varphi \\ \sin\varphi \end{pmatrix}, \tag{A11}$$

$$\lambda_v = +\frac{\mathcal{A}_\perp}{2}, \quad \hat{\vec{v}}_\perp = \begin{pmatrix} -\sin\varphi \\ \cos\varphi \end{pmatrix}, \tag{A12}$$

where the hats emphasize that these are unit vectors. We observe that the relative phase of the ψ_1 and ψ_{-1} components directly determines the orientation φ of the planar director $\vec{u}_\perp$. Note that this result is general for any spin-1 spinor, however, for the particular case of the EP ground state, (27), we have $\varphi \to \phi$, $\mathcal{A}_\perp \to n_c$.

APPENDIX B: CORRELATION FUNCTIONS

Using the results in the previous section we can provide an alternative motivation for the correlation functions used in the paper. First, we consider the orientation of the director at two points in space. For a spin model this might be characterized by a correlation function of the form

$$G_u(\mathbf{r}) = \langle|\hat{\vec{u}}(\mathbf{0}) \cdot \hat{\vec{u}}(\mathbf{r})|^2\rangle = \tfrac{1}{2}\langle\cos(2[\varphi(\mathbf{0}) - \varphi(\mathbf{r})]) + 1\rangle, \tag{B1}$$

where the inner product is squared to account for $\vec{u}$ and $-\vec{u}$ being the same. In terms of the fields our relevant quantity is the complex density $\Phi \equiv \psi_1^*\psi_{-1} = \frac{1}{2}\mathcal{A}_\perp e^{2i\varphi}$. Correlating this at two points in space we have

$$G_\Phi(\mathbf{r}) = \langle\Phi(\mathbf{0})\Phi^*(\mathbf{r})\rangle \tag{B2}$$

$$= \langle\psi_1^*(\mathbf{0})\psi_{-1}(\mathbf{0})\psi_{-1}^*(\mathbf{r})\psi_1(\mathbf{r})\rangle, \tag{B3}$$

which is identical to G_ϕ as defined in (25) if we normalize by a factor of $4/n_c^2$.

From Eqs. (A2) and (A5) we see that the superfluid phase $\theta_\perp$ is related to the singlet amplitude as

$$\alpha_\perp = -2\psi_1\psi_{-1} = -\mathcal{A}_\perp e^{2i\theta_\perp}, \tag{B4}$$

where we can take $\theta_\perp = \frac{1}{2}\mathrm{Arg}(\psi_1\psi_{-1})$. Thus to correlate this superfluid order at two points we can consider the pairinglike field $\alpha_\perp$ at these two locations, i.e.,

$$G_{\alpha_\perp}(\mathbf{r}) = \langle\alpha_\perp^*(\mathbf{0})\alpha_\perp(\mathbf{r})\rangle, \tag{B5}$$

$$= 4\langle\psi_1^*(\mathbf{0})\psi_{-1}^*(\mathbf{0})\psi_{-1}(\mathbf{r})\psi_1(\mathbf{r})\rangle. \tag{B6}$$

Normalizing by a factor of n_c^{-2} gives G_θ [Eq. (26)].

[1] J. Stenger, S. Inouye, D. M. Stamper-Kurn, H.-J. Miesner, A. P. Chikkatur, and W. Ketterle, Nature **396**, 345 (1998).
[2] T.-L. Ho, Phys. Rev. Lett. **81**, 742 (1998).
[3] T. Ohmi and K. Machida, J. Phys. Soc. Jpn. **67**, 1822 (1998).
[4] Y. Kawaguchi and M. Ueda, Phys. Rep. **520**, 253 (2012).
[5] T. Zibold, V. Corre, C. Frapolli, A. Invernizzi, J. Dalibard, and F. Gerbier, Phys. Rev. A **93**, 023614 (2016).
[6] H. Orihara and Y. Ishibashi, J. Phys. Soc. Jpn. **55**, 2151 (1986).
[7] I. Chuang, N. Turok, and B. Yurke, Phys. Rev. Lett. **66**, 2472 (1991).
[8] I. Chuang, R. Durrer, N. Turok, and B. Yurke, Science **251**, 1336 (1991).
[9] B. Yurke, A. N. Pargellis, and N. Turok, Mol. Cryst. Liq. Cryst. Sci. Technol., Sec. A **222**, 195 (1992).
[10] T. Nagaya, H. Hotta, H. Orihara, and Y. Ishibashi, J. Phys. Soc. Jpn. **61**, 3511 (1992).
[11] R. E. Blundell and A. J. Bray, Phys. Rev. A **46**, R6154 (1992).
[12] I. Chuang, B. Yurke, A. N. Pargellis, and N. Turok, Phys. Rev. E **47**, 3343 (1993).

[13] S. Mukerjee, C. Xu, and J. E. Moore, Phys. Rev. B **76**, 104519 (2007).
[14] K. Kudo and Y. Kawaguchi, Phys. Rev. A **88**, 013630 (2013).
[15] K. Kudo and Y. Kawaguchi, Phys. Rev. A **91**, 053609 (2015).
[16] L. A. Williamson and P. B. Blakie, Phys. Rev. Lett. **116**, 025301 (2016).
[17] E. M. Bookjans, A. Vinit, and C. Raman, Phys. Rev. Lett. **107**, 195306 (2011).
[18] A. Vinit, E. M. Bookjans, C. A. R. S. de Melo, and C. Raman, Phys. Rev. Lett. **110**, 165301 (2013).
[19] N. T. Phuc, Y. Kawaguchi, and M. Ueda, Phys. Rev. A **88**, 043629 (2013).
[20] J. Jiang, L. Zhao, M. Webb, and Y. Liu, Phys. Rev. A **90**, 023610 (2014).
[21] A. Vinit and C. Raman, Phys. Rev. A **95**, 011603 (2017).
[22] A. Bourges and P. B. Blakie, Phys. Rev. A **95**, 023616 (2017).
[23] S. W. Seo, S. Kang, W. J. Kwon, and Y.-I. Shin, Phys. Rev. Lett. **115**, 015301 (2015).
[24] S. W. Seo, W. J. Kwon, S. Kang, and Y. Shin, Phys. Rev. Lett. **116**, 185301 (2016).
[25] J. Lovegrove, M. O. Borgh, and J. Ruostekoski, Phys. Rev. A **86**, 013613 (2012).
[26] I. Carusotto and E. J. Mueller, J. Phys. B **37**, S115 (2004).
[27] J. M. Higbie, L. E. Sadler, S. Inouye, A. P. Chikkatur, S. R. Leslie, K. L. Moore, V. Savalli, and D. M. Stamper-Kurn, Phys. Rev. Lett. **95**, 050401 (2005).
[28] D. Baillie and P. B. Blakie, Phys. Rev. A **93**, 033607 (2016).
[29] M. Karl, B. Nowak, and T. Gasenzer, Phys. Rev. A **88**, 063615 (2013).
[30] F. Gerbier, A. Widera, S. Fölling, O. Mandel, and I. Bloch, Phys. Rev. A **73**, 041602 (2006).
[31] S. R. Leslie, J. Guzman, M. Vengalattore, J. D. Sau, M. L. Cohen, and D. M. Stamper-Kurn, Phys. Rev. A **79**, 043631 (2009).
[32] E. J. Mueller, Phys. Rev. A **69**, 033606 (2004).
[33] E. Yukawa and M. Ueda, Phys. Rev. A **86**, 063614 (2012).
[34] Note that our definition differs by a constant factor from [4].
[35] The z magnetization $M_z \equiv \int d^2\mathbf{x} F_z$ of the system is conserved, and here we focus on the case $M_z = 0$, where the transition occurs at $q = 0$.
[36] S. Kang, S. W. Seo, J. H. Kim, and Y.-I. Shin, Phys. Rev. A **95**, 053638 (2017).
[37] E. Witkowska, T. Świsłocki, and M. Matuszewski, Phys. Rev. A **90**, 033604 (2014).
[38] P. G. de Gennes and J. Prost, *The Physics of Liquid Crystals*. *International Series of Monographs on Physics* (Clarendon Press, Gloucestershire, UK, 1995).
[39] $\mathcal{A}_\perp$ is sensitive to the anisotropy of Q but does not completely distinguish between polar and ferromagnetic states as does $\mathcal{A}$. For example, the fully ferromagnetic state with $\mathbf{F} = n\hat{\mathbf{x}}$ has $\mathcal{A} = 0$ but $\mathcal{A}_\perp = \frac{1}{2}n$ (cf. the pure EP polar state with $\vec{u} = \sqrt{n}\hat{\mathbf{x}}$, for which $\mathcal{A} = \mathcal{A}_\perp = n$). As is apparent from Fig. 1(a), a state with $\mathbf{F} \neq 0$ also has an anisotropic nematic tensor, just to a lesser extent than a polar state.
[40] L. E. Sadler, J. M. Higbie, S. R. Leslie, M. Vengalattore, and D. M. Stamper-Kurn, Nature **443**, 312 (2006).
[41] L. M. Symes, R. I. McLachlan, and P. B. Blakie, Phys. Rev. E **93**, 053309 (2016).
[42] P. B. Blakie, A. S. Bradley, M. J. Davis, R. J. Ballagh, and C. W. Gardiner, Adv. Phys. **57**, 363 (2008).
[43] L. A. Williamson and P. B. Blakie, Phys. Rev. A **94**, 023608 (2016).
[44] H. Saito, Y. Kawaguchi, and M. Ueda, Phys. Rev. A **76**, 043613 (2007).
[45] A. Lamacraft, Phys. Rev. Lett. **98**, 160404 (2007).
[46] R. Barnett, A. Polkovnikov, and M. Vengalattore, Phys. Rev. A **84**, 023606 (2011).
[47] J. Guzman, G.-B. Jo, A. N. Wenz, K. W. Murch, C. K. Thomas, and D. M. Stamper-Kurn, Phys. Rev. A **84**, 063625 (2011).
[48] Here and for the remainder of this subsection all expectations are taken to be spatially averaged as in Eq. (19).
[49] A. J. Bray, Adv. Phys. **43**, 357 (1994).
[50] Domain size cannot be uniquely defined because the in-plane nematic order varies continuously.
[51] B. Yurke, A. N. Pargellis, T. Kovacs, and D. A. Huse, Phys. Rev. E **47**, 1525 (1993).
[52] A. J. Bray, A. J. Briant, and D. K. Jervis, Phys. Rev. Lett. **84**, 1503 (2000).
[53] M. Kulczykowski and M. Matuszewski, Phys. Rev. B **95**, 075306 (2017).
[54] A. N. Pargellis, P. Finn, J. W. Goodby, P. Panizza, B. Yurke, and P. E. Cladis, Phys. Rev. A **46**, 7765 (1992).
[55] K. Nam, B. Kim, and S. J. Lee, J. Stat. Mech. (2011) P03013.
[56] A. Singh, S. Ahmad, S. Puri, and S. Singh, Europhys. Lett. **100**, 36004 (2012).
[57] A. Singh and S. Singh, Eur. Phys. J. E **36**, 122 (2013).
[58] L. A. Williamson and P. B. Blakie, arXiv:1703.09360.
[59] A. J. Bray and S. Puri, Phys. Rev. Lett. **67**, 2670 (1991).
[60] P. Öhberg and L. Santos, Phys. Rev. A **66**, 013616 (2002).
[61] M. Eto, K. Kasamatsu, M. Nitta, H. Takeuchi, and M. Tsubota, Phys. Rev. A **83**, 063603 (2011).
[62] K. Kasamatsu, M. Eto, and M. Nitta, Phys. Rev. A **93**, 013615 (2016).
[63] A.-C. Ji, W. M. Liu, J. L. Song, and F. Zhou, Phys. Rev. Lett. **101**, 010402 (2008).
[64] W. E. Shirley, B. M. Anderson, C. W. Clark, and R. M. Wilson, Phys. Rev. Lett. **113**, 165301 (2014).
[65] A. M. Turner, Phys. Rev. Lett. **103**, 080603 (2009).
[66] L. A. Williamson and P. B. Blakie, Phys. Rev. A **94**, 063615 (2016).
[67] This mapping is made by neglecting the ψ_0 component in the spin-1 GPE.
[68] J. Schole, B. Nowak, and T. Gasenzer, Phys. Rev. A **86**, 013624 (2012).
[69] M. O. Borgh and J. Ruostekoski, Phys. Rev. Lett. **109**, 015302 (2012).
[70] M. O. Borgh, J. Lovegrove, and J. Ruostekoski, New J. Phys. **16**, 053046 (2014).